

Change of the shape of mass and charge distributions in fission of Cf isotopes with excitation energy

H. Paşca,^{1,2} A. V. Andreev,³ G. G. Adamian,³ and N. V. Antonenko^{3,4}

¹Joint Institute for Nuclear Research, 141980 Dubna, Russia

²“Babeş-Bolyai” University, Faculty of Physics, 400084 Cluj-Napoca, Romania

³Joint Institute for Nuclear Research, 141980 Dubna, Russia

⁴Mathematical Physics Department, Tomsk Polytechnic University, 634050 Tomsk, Russia



(Received 24 January 2019; published 17 June 2019)

Using the improved scission-point model, the mass and charge distributions of fragments resulting from the fission of californium isotopes are calculated and compared with the available experimental data. The change of the shape of mass and charge distributions with increasing excitation energy is predicted for future experiments.

DOI: [10.1103/PhysRevC.99.064611](https://doi.org/10.1103/PhysRevC.99.064611)

I. INTRODUCTION

There is a longstanding opinion that the competition between symmetric and asymmetric fission modes is mainly related to the deformed shells [1]. However, in the case of neutron-induced fission of ^{238}U , the recent experimental data [2] have shown that the mass distribution maintains two-peaked shape even at neutron energies of $E_n = 50\text{--}60$ MeV. The asymmetric peaks in $^{232}\text{Th}(n, f)$ at $E_n = 50\text{--}70$ MeV have been reported in Ref. [3]. The same effect was observed in Refs. [4–6]. The presence of a strong asymmetric component in the multinucleon transfer-induced fission of ^{244}Cm at $E^* = 23$ MeV and ^{250}Cf at $E^* = 46$ MeV has been recently observed in Refs. [7–9]. Asymmetric shapes of the mass distribution resulting from the fission of highly excited nuclei $^{237\text{--}240}\text{U}$, $^{239\text{--}242}\text{Np}$, and $^{241\text{--}244}\text{Pu}$ (the excitation energies $E^* \approx 0\text{--}70$ MeV), originating from the transfer reaction $^{18}\text{O} + ^{238}\text{U}$ at $E_{\text{lab}} = 157.5$ MeV, have been experimentally observed in Refs. [10,11]. Different angular momentum distributions of the produced compound nucleus are expected from transfer and neutron-capture reactions. However, the transfer-induced fission data are comparable to fission data caused by fast neutrons, which means that rotation has minor effect on the fragment mass distribution [7–9]. At the excitation energies 50–70 MeV, the shell effects are expected to be washed out, and the nucleus is supposed to leave with a dominant symmetric mode, which is contrary to the experiments. Thus, the statement that with increasing excitation energy the shell effects melt always leaves the fissioning nucleus with a dominant symmetric mode is not completely correct. The possible reason(s) for that could be the underestimation of the roles of shell and/or macroscopic effects. Because the shell effects are very important for the description of fission properties of heaviest actinides, it is interesting to study the excitation energy dependence of the fission observables in these nuclei. Note that the multichance fission of $E^* > 50$ MeV can not explain [14] the presence of asymmetric mode in the experiments mentioned.

In the present paper we will study the evolution of charge and mass distributions of fission fragments with increasing excitation energy in even-even $^{248\text{--}254}\text{Cf}$ isotopes. As known, in $^{250}\text{Cf}(s.f.)$ and $^{249}\text{Cf}(n_{\text{th}}, f)$ the charge distribution is two peaked. For $^{250,252,254,256}\text{Cf}(s.f.)$ and $^{249,251}\text{Cf}(n_{\text{th}}, f)$, the mass distribution is also asymmetric [12,13,15]. Our aim is to predict the charge and mass distributions at large excitation energies. The fission observables are described using the improved scission-point model [16–19]. The statistical scission-point model [16–19] relies on the assumption that the statistical equilibrium is established at touching configuration where the observable characteristics of fission process are formed. The reliability of this conclusion is supported by a good description of various experimental data (mass, charge, kinetic energy distributions, and neutron multiplicity) with the scission-point-type models [16–28].

II. MODEL

The most important step of the statistical scission-point model is the calculation of the potential energy of the system as a function of charge Z_i , mass A_i , deformations β_i (the ratios between the major and minor semiaxes of the fragments) of the two fission fragments, and internuclear distance R between them. The index i designates the light (L) or heavy (H) fission fragment. The scission configuration is imagined as two axially deformed and uniformly charged spheroids—the nascent fission fragments. The two nuclei are fully formed and possess all the features of isolated nuclei, e.g., binding energies, according to the separability principle [29], and mutually interact through the nuclear and Coulomb forces. Their orientation is frozen to a tip-to-tip configuration, which provides the minimum interaction energy. Owing to the repulsive nature of the Coulomb interaction V^C and attractive nature of the nuclear interaction V^N , a potential pocket is formed in the R coordinate, which corresponds roughly to a separation of 0.5–1.1 fm between the tips of

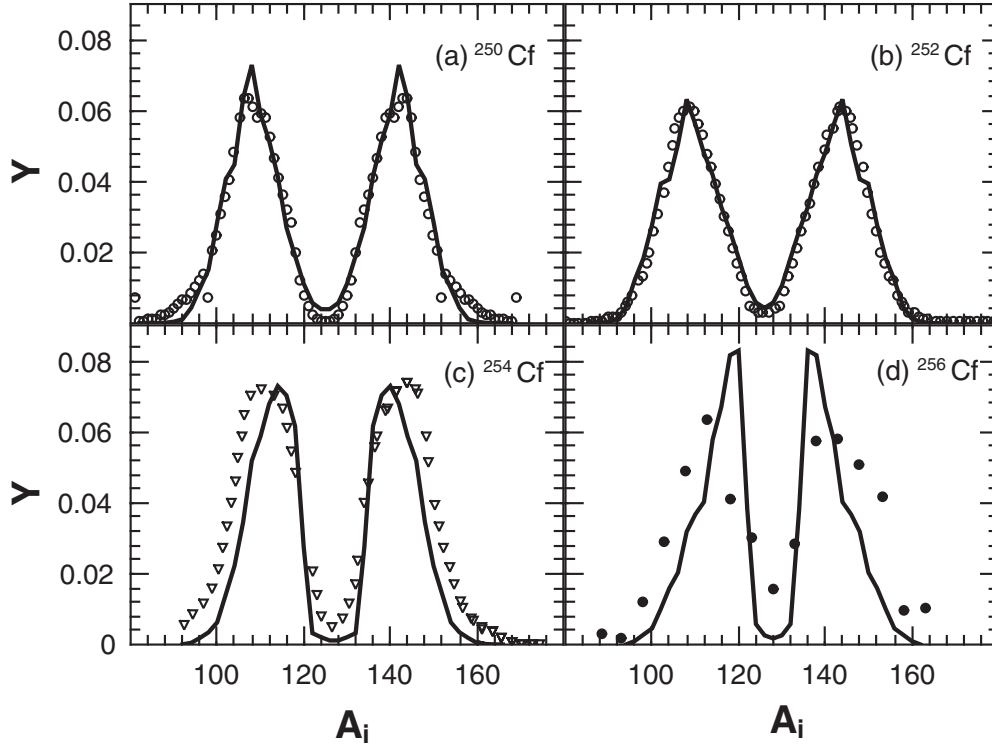


FIG. 1. The calculated (lines) mass distributions of fragments resulting from the spontaneous fission of $^{250,252,254,256}\text{Cf}$ are compared with the available experimental data (symbols) [12,13,32,33]. The calculations are performed for the even-even mass and charge fragmentations. The distributions are normalized to unity.

the fragments, depending on the mass $A_{L,H}$ and charge $Z_{L,H}$ numbers, and deformations $\beta_{L,H}$. Because of the assumption of the model that statistical equilibrium is achieved at the scission point, one can reduce the complexity of the problem by fixing the internuclear distance at the bottom of the potential pocket ($R = R_m$). One should keep in mind that the depth of the potential pocket (the decay barrier B_{qf}) varies with charge asymmetry and/or deformation of the fragments, being smaller for charge-symmetric fragments and/or highly elongated nuclei, and deeper for asymmetric fragments and/or spherical-nuclei.

The potential energy

$$\begin{aligned}
 U(A_i, Z_i, \beta_i, R_m) &= U_L^{\text{LD}}(A_L, Z_L, \beta_L, E_L^*) + \delta U_L^{\text{shell}}(A_L, Z_L, \beta_L, E_L^*) \\
 &+ U_H^{\text{LD}}(A_H, Z_H, \beta_H, E_H^*) + \delta U_H^{\text{shell}}(A_H, Z_H, \beta_H, E_H^*) \\
 &+ V^C(A_i, Z_i, \beta_i, R_m) + V^N(A_i, Z_i, \beta_i, R_m) \quad (1)
 \end{aligned}$$

of the system is calculated as the sum the energies of the fragments [the liquid-drop (LD) energy U_i^{LD} plus shell-correction term $\delta U_i^{\text{shell}}$] and energy $V = V^C + V^N$ of the fragment-fragment interaction [16–19]. The interaction potential consists of the Coulomb interaction potential V^C of two uniformly charged ellipsoids and nuclear interaction potential in the double-folding form [30].

$$V^N = \int \rho_L(\mathbf{r}_1)\rho_H(\mathbf{R} - \mathbf{r}_2)F(\mathbf{r}_1 - \mathbf{r}_2)d\mathbf{r}_1d\mathbf{r}_2, \quad (2)$$

in the form of the double folding of Woods-Saxon nuclear densities ρ_i of the fragments and Skyrme-type density-dependent nucleon-nucleon interaction

$$F(\mathbf{r}_1 - \mathbf{r}_2) = C_0 \left[F_{\text{in}} \frac{\rho_0(\mathbf{r}_1)}{\rho_{00}} + F_{\text{ex}} \left(1 - \frac{\rho_0(\mathbf{r}_1)}{\rho_{00}} \right) \right] \delta(\mathbf{r}_1 - \mathbf{r}_2),$$

where $\rho_0(\mathbf{r}) = \rho_L(\mathbf{r}) + \rho_H(\mathbf{R} - \mathbf{r})$, $F_{\text{in},\text{ex}} = f_{\text{in},\text{ex}} + f'_{\text{in},\text{ex}} \frac{(N_L - Z_L)(N_H - Z_H)}{(N_L + Z_L)(N_H + Z_H)}$, $C_0 = 300 \text{ MeV fm}^3$, $f_{\text{in}} = 0.09$, $f_{\text{ex}} = -2.59$, $f'_{\text{in}} = 0.42$, $f'_{\text{ex}} = -0.54$, and $\rho_{00} = 0.17 \text{ fm}^{-3}$. The nuclear densities are taken in the two-parameter Fermi form with the diffuseness parameter $a = 0.51\text{--}0.56 \text{ fm}$ depending on the charge number of the nucleus. The symmetry, Coulomb and surface parts of LD energy are calculated as

$$\begin{aligned}
 U_i^{\text{sym}}(A_i, Z_i, E_i^*) &= 27.612 \frac{(N_i - Z_i)^2}{A_i} [1 + 6 \times 10^{-4} E_i^*/A_i], \\
 U_i^C(A_i, Z_i, \beta_i, E_i^*) &= \frac{3 Z_i^2 e^2}{5 R_{0i}} \frac{\beta_i^{1/3}}{\sqrt{\beta_i^2 - 1}} \\
 &\times \ln [\beta_i + \sqrt{\beta_i^2 - 1}] [1 - 0.12 E_i^*/A_i], \\
 U_i^{\text{sur}}(A_i, Z_i, \beta_i, E_i^*) &= \sigma_i S_i [1 + 0.102 E_i^*/A_i], \quad (3)
 \end{aligned}$$

where E_i^* are the excitation energies of fragments, $R_{0i} = 1.2249 A_i^{1/3} \text{ fm}$, the area S_i of nuclear surface and the deformation-dependent surface tension coefficient $\sigma_i = \sigma_{0i} [1 + k_i (\beta_i - \beta_i^{s.s.})^2] f(Z_i)$, $\sigma_{0i} = 0.9517 [1 - 1.7826$

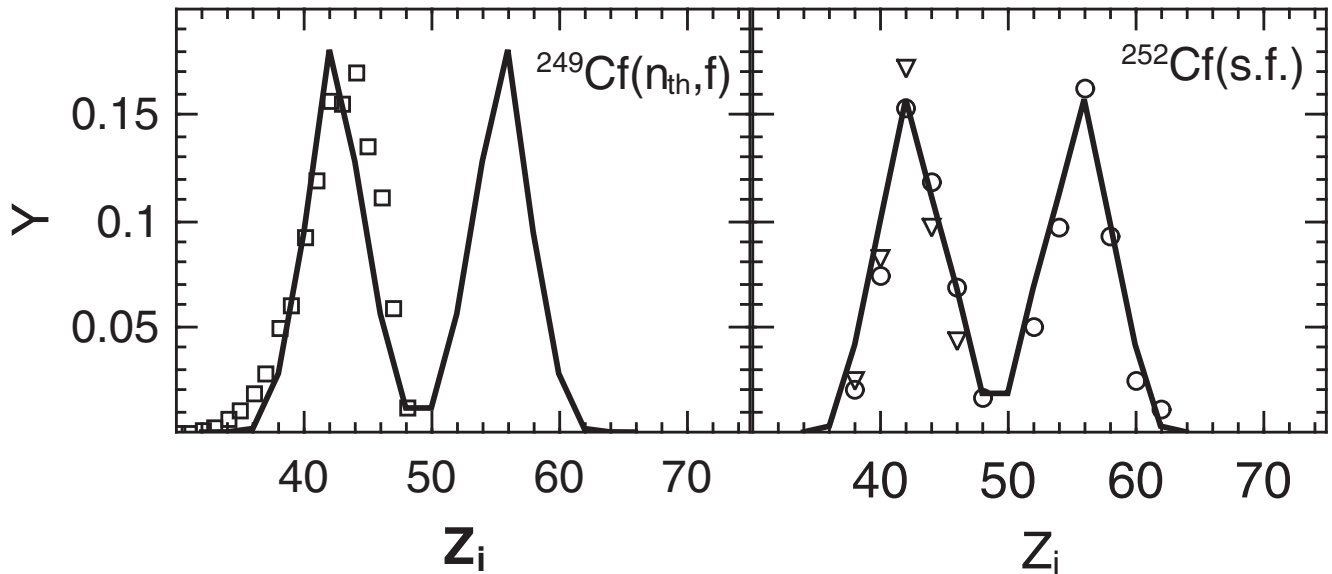


FIG. 2. The calculated (lines) charge distributions of fragments resulting from the thermal-neutron induced fission of ^{249}Cf and the spontaneous fission of ^{250}Cf are compared with the available experimental data (symbols) [34,35]. The calculations are performed for the even-even mass and charge fragmentations.

$(N_i - Z_i)^2/A_i^2$], $f(Z_i) = 1 - 0.00025(Z_i - Z_r)^2$, $Z_r = Z/2 - [15.55 - 0.25(N - Z)]$, and stiffness coefficient $k_i(E_i^*) = \frac{0.06 \exp(-E_i^*/3.7)}{1 + \exp(-0.063[C_{\text{vib}}(Z_i, A_i) - 67])}$. Here, $\beta_i^{g.s.}$ and $C_{\text{vib}}(Z_i, A_i)$ are the ground-state deformation and stiffness of the nucleus, respectively [25]. The excitation energy dependence of the liquid-drop terms is taken in a similar way as in Ref. [31].

The shell-correction terms are calculated with the Strutinsky method and the two-center shell model [29]. The damping of the shell corrections with excitation energy E_i^* is

introduced as

$$\begin{aligned} \delta U_i^{\text{shell}}(A_i, Z_i, \beta_i, E_i^*) \\ = \delta U_i^{\text{shell}}(A_i, Z_i, \beta_i, E_i^* = 0) \exp[-E_i^*/E_D], \end{aligned} \quad (4)$$

where $E_D = 18.5$ MeV is the damping constant. The excitation energy is assumed to be shared between the fragments proportional to their masses. This is rather good approximation for the fragmentations and excitation energies considered.

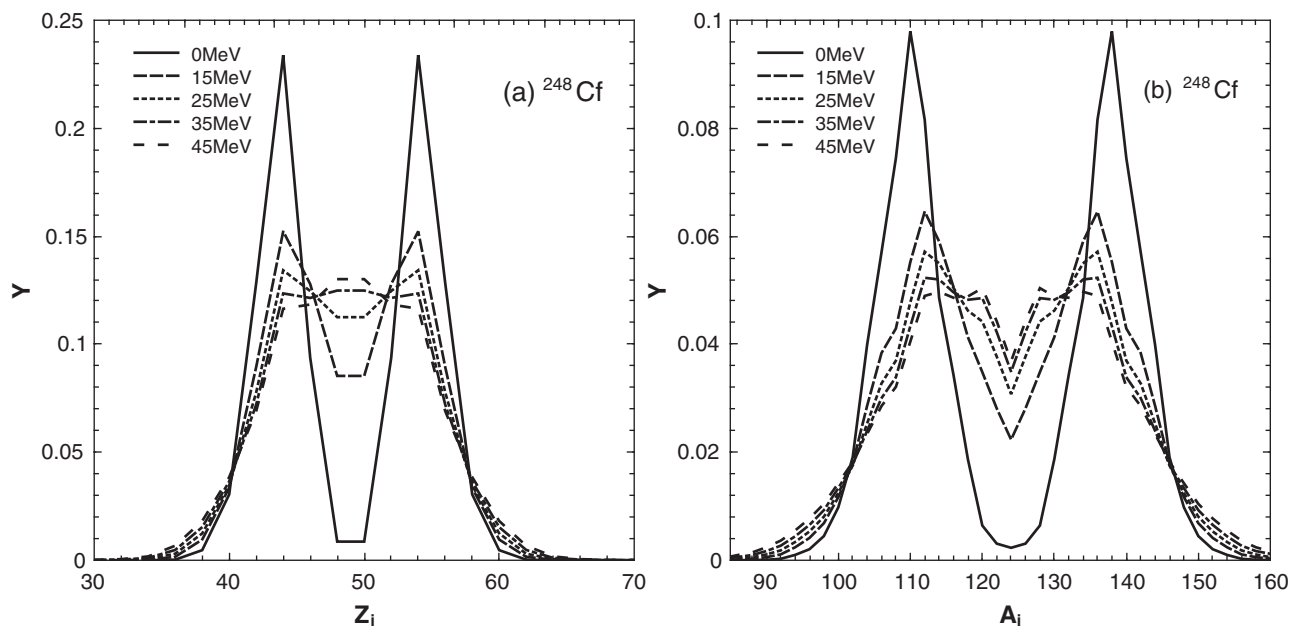


FIG. 3. The calculated (a) charge and (b) mass distributions of fragments resulting from the fission of ^{248}Cf at indicated excitation energies. The calculations are performed for the even-even mass and charge fragmentations.

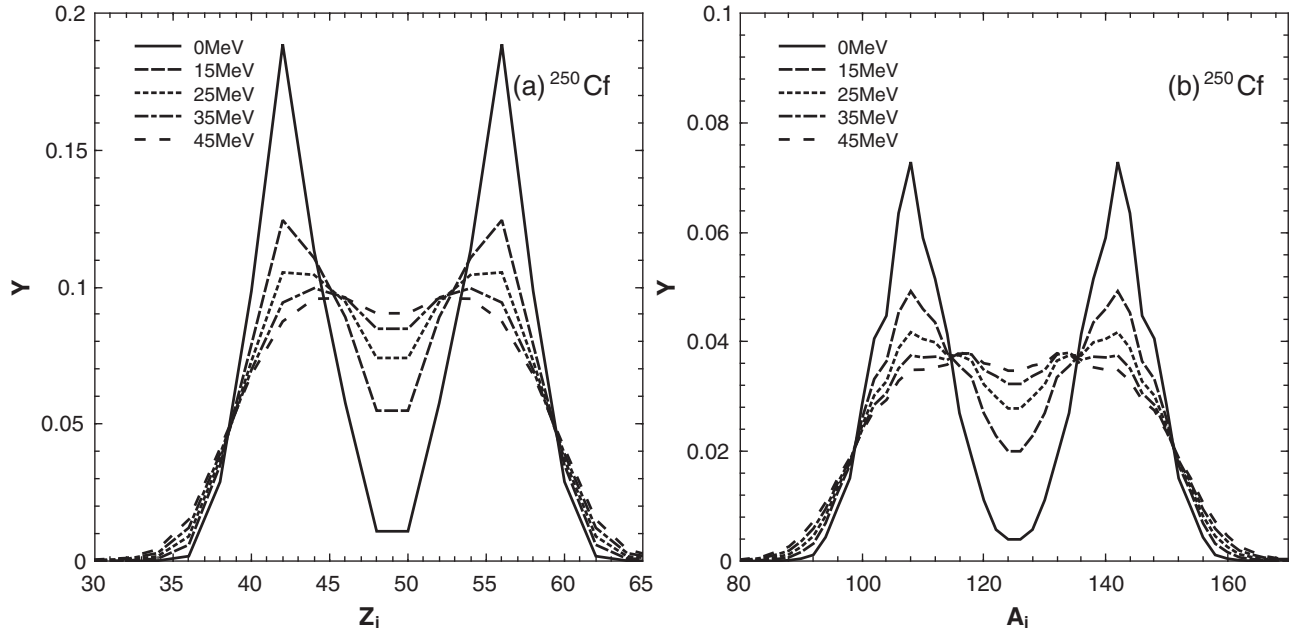


FIG. 4. The same as in Fig. 3, but for the fission of ^{250}Cf .

Because the thermal equilibrium is assumed at scission point, the relative formation probability of the DNS with particular masses, charges, and deformations of the fragments is statistically calculated as follows:

$$w(A_i, Z_i, \beta_i, E^*) = N_0 \exp \left[-\frac{U(A_i, Z_i, \beta_i, R_m) + B_{qf}(A_i, Z_i, \beta_i)}{T} \right], \quad (5)$$

where N_0 is the normalization factor. In Eq. (5), the temperature is calculated as $T = \sqrt{E_{\text{DNS}}^*/a}$, where E_{DNS}^* is the excitation energy of the dinuclear system at the unconditional minimum of U and $a = A/12 \text{ MeV}^{-1}$ is the level

density parameter in the Fermi-gas model. In the calculations of the yields, we use a single value of T , which corresponds to the global minimum of the potential energy surface, before the shell damping. As seen, the decay barrier B_{qf} , calculated as the difference of the potential energies at the bottom of the potential pocket ($R = R_m$) and at the top of the external barrier [located at the distance $R = R_b$ of about (1.5–2) fm between the tips of fragments], has also an impact on the yields. The term $\exp[-B_{qf}/T]$ describes the thermal penetration of the decay barrier. With increasing elongation and decreasing charge (mass) asymmetry the value of B_{qf} decreases, the system becomes more unstable and decays. We use an indirect shape restriction, which is connected to the

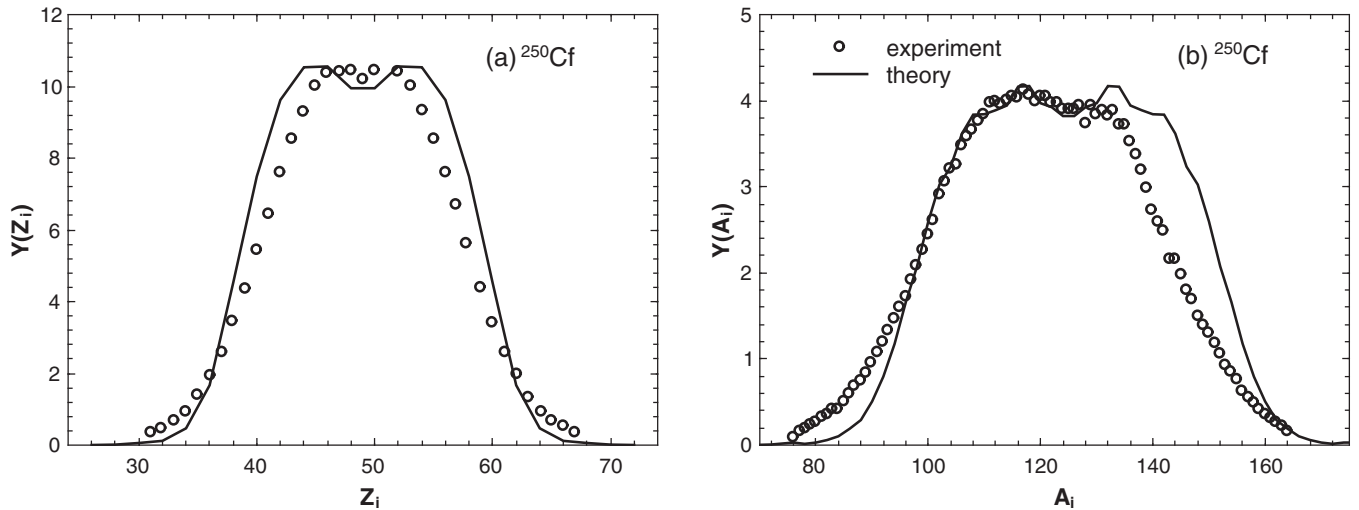
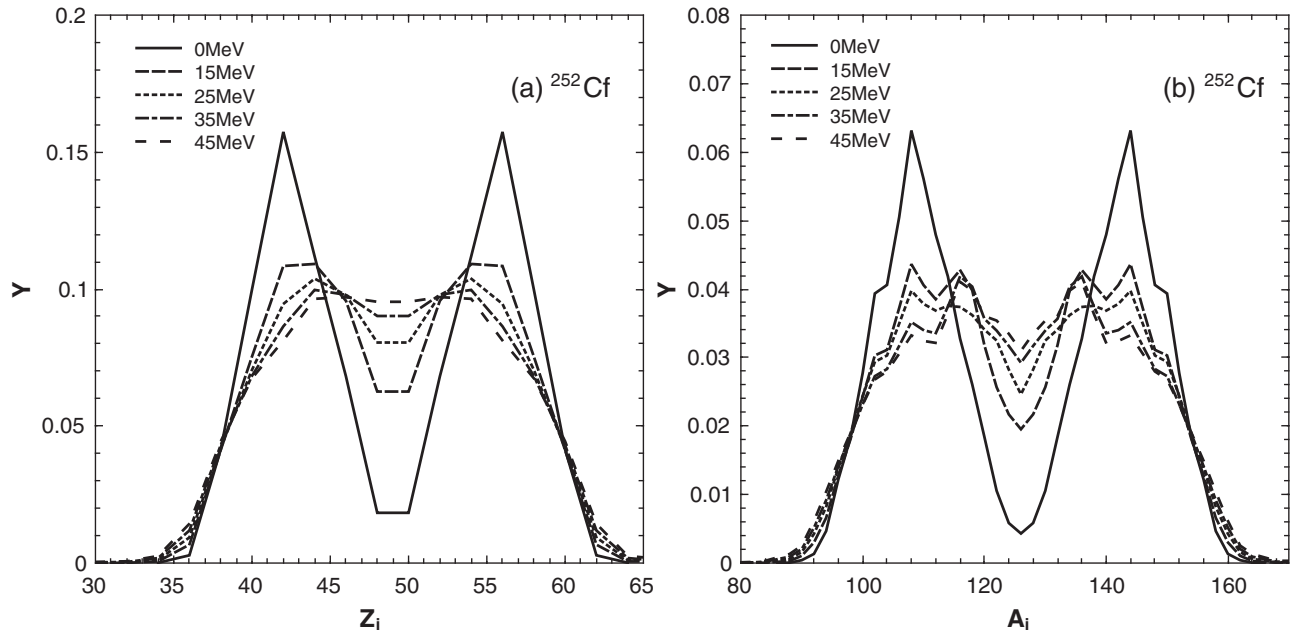


FIG. 5. For the fission of highly excited ^{250}Cf nucleus ($E^* = 46 \text{ MeV}$), the calculated (lines) primary (a) charge and (b) mass distributions are compared with the measured secondary charge and mass distributions (symbols) [9]. The calculations are performed for the even-even mass and charge fragmentations.

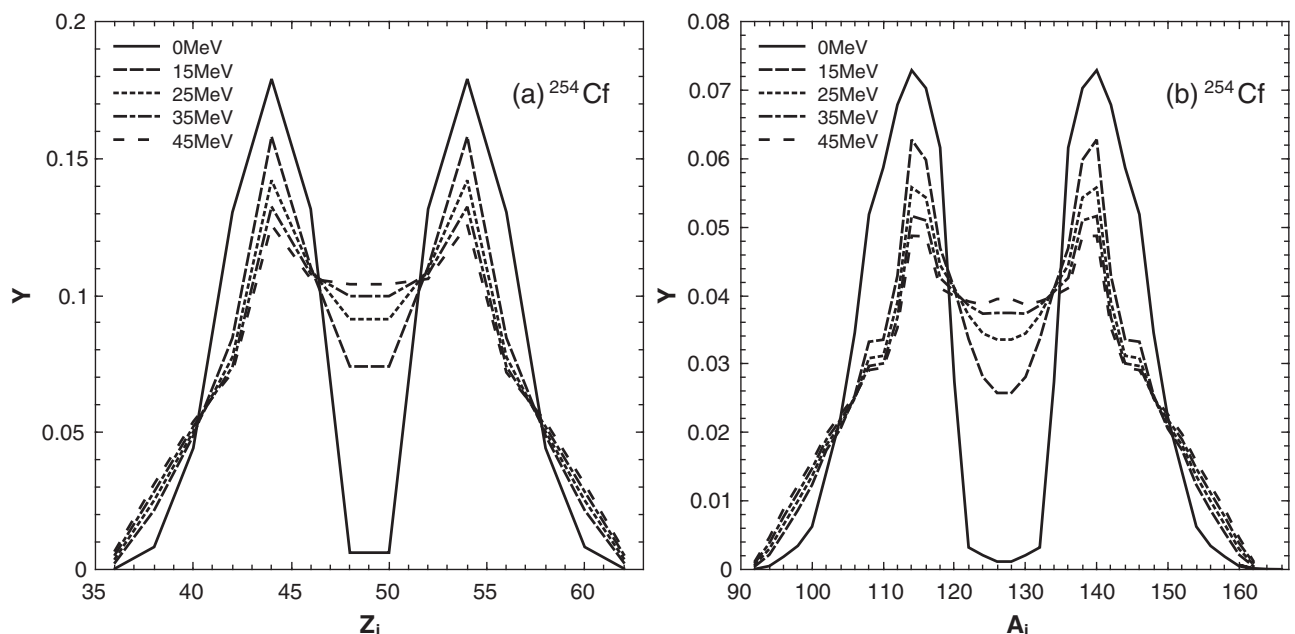
FIG. 6. The same as in Fig. 3, but for the fission of ^{252}Cf .

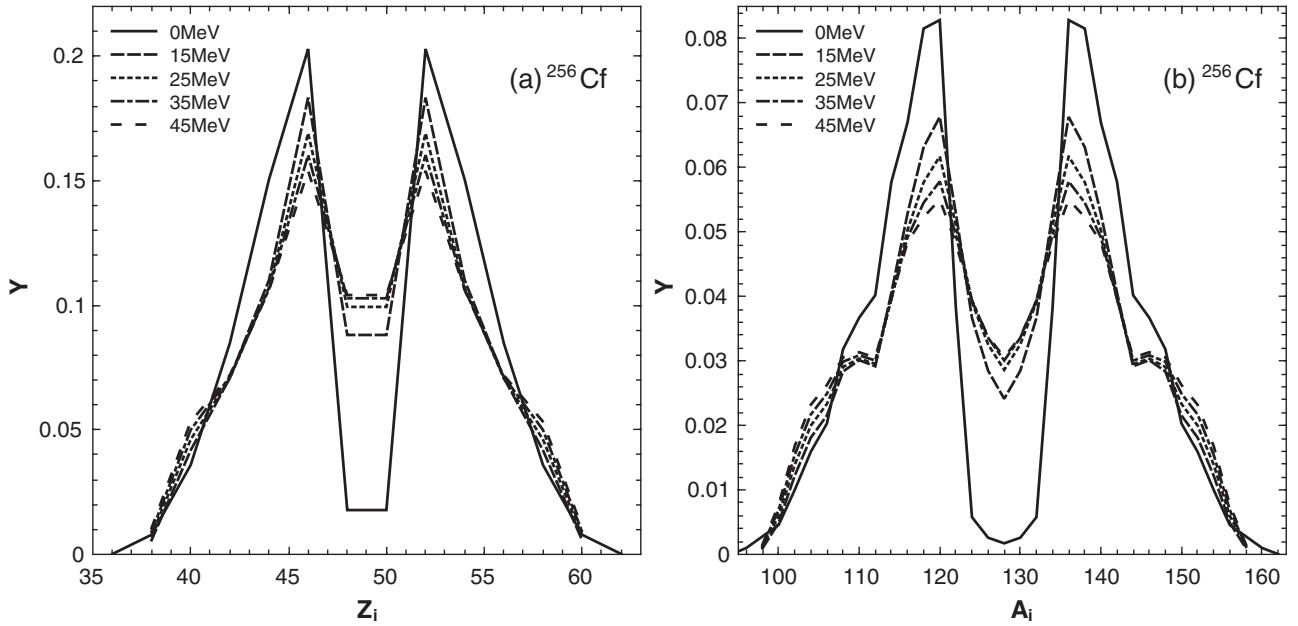
value of the decay barrier B_{qf} at the scission point. Thus, we take into account only those configurations for which B_{qf} is larger than a minimum value $B_{qf}^m \approx 0.1$ MeV to ensure that unrealistic, highly deformed configurations are excluded. A reasonable variation of the parameter B_{qf}^m leads only to not strong change of the width of the mass (charge) distribution. For example, at $B_{qf}^m = 0$, the fission-mode distribution is narrow, whereas at $B_{qf}^m = 0.3$ MeV, the distribution is wide with respect to the distribution at $B_{qf}^m = 0.1$ MeV. So, our conclusion about the asymmetry of the shape of the mass and charge distributions is not sensitive to the variation of B_{qf}^m .

In order to obtain the mass-charge distribution of fission fragments, one should integrate (5) over β_L and β_H :

$$Y(A_i, Z_i, E^*) = \int d\beta_L d\beta_H w(A_i, Z_i, \beta_i, E^*). \quad (6)$$

The ratio of the yields of fragments with different charge/mass numbers is mainly governed by the difference in energy between the corresponding potential minima in the plane (β_L, β_H) , as seen in Eq. (5). For two potential energy surfaces with the minima, which are close in energy, a higher yield stems from the DNS with a wider and shallower

FIG. 7. The same as in Fig. 3, but for the fission of ^{254}Cf .

FIG. 8. The same as in Fig. 3, but for the fission of ^{256}Cf .

minimum, and lower yield emerges from an abrupt and narrow minimum. This is a direct result of Eq. (6) [17,27]. Note that in the case of fast (slow) growth of the liquid-drop surface energy with increasing deformations, the minimum in the (β_L, β_H) plane is positioned at smaller (larger) deformations and is deep and narrow (shallow and wide). Finally, for the calculation of the charge (mass) distributions, one should sum Eq. (6) over the mass (charge) numbers:

$$Y(Z_i) = \sum_{A_i} \int d\beta_L d\beta_H w(A_i, Z_i, \beta_i, E^*), \quad (7)$$

$$Y(A_i) = \sum_{Z_i} \int d\beta_L d\beta_H w(A_i, Z_i, \beta_i, E^*). \quad (8)$$

Additionally, various average quantities can be calculated using the prescription described. For example, the average charge and mass numbers of the light fission fragment are

$$\langle Z \rangle = \sum_{Z_i} Z_i Y(Z_i), \quad (9)$$

$$\langle A \rangle = \sum_{Z_i} A_i Y(A_i). \quad (10)$$

III. RESULTS AND DISCUSSIONS

In Fig. 1, the calculated mass distributions of fragments resulting from the spontaneous fission of even-even nuclei $^{250-256}\text{Cf}$ are compared with the existing experimental data [12,13,32,33]. For the fissioning nuclei $^{254,256}\text{Cf}$, the experimental data [32,33] correspond to the preneutron emission mass yields. In Fig. 2, the charge distributions of fragments are the result of thermal-neutron induced fission $^{249}\text{Cf}(n_{\text{th}}, f)$ and spontaneous fission of ^{252}Cf . As seen in Figs. 1 and 2, our calculations agree well with the experimental data. The asymmetric nature of the mass distributions of fragments is evident

in the spontaneous and thermal-neutron-induced fission of Cf isotopes. For example, the maxima of charge and mass yields in $^{249}\text{Cf}(n_{\text{th}}, f)$ and $^{252}\text{Cf}(s.f.)$ are at $Z_L = 42$ and $A_L = 108$, respectively. It is worth mentioning the small increase of the calculated yields near symmetry with decreasing neutron number of the fissioning nucleus interaction potential, which promotes the high yields. The same behavior is observed, for example, in the electromagnetic-induced fission of neutron-deficient U isotopes [27].

In Figs. 3–10, the predicted charge and mass distributions of fragments resulting from the fission of the excited even-even isotopes $^{248-256}\text{Cf}$ are presented. Some general noteworthy aspects are observed. For the isotopes of Cf with increasing excitation energy, almost symmetric components (Cd + Sn) of the mass and charge distributions are enhanced with respect to the asymmetric components Mo + Ba and Ru + Xe. The fast evolution of the symmetric yields is found with increasing excitation energy from 0 to (15–25) MeV. The saturation of the symmetric components is reached at about of $E^* = 55$ MeV. At excitation energy 45 MeV, the asymmetric shape of the distributions is preserved, being more pronounced in the mass distributions. The charge distribution in the fission of ^{248}Cf shows the formation of a small almost symmetric peak with charge split Cd + Sn. At the highest excitation energies 55 and 65 MeV, the fission of $^{252,254,256}\text{Cf}$ has the asymmetric mass yields, being less pronounced with the reduction of neutron number in the fissioning nucleus. For the fission of the ^{250}Cf at $E^* = 55$ and 65 MeV, the mass distribution has the quasi-Gaussian shape with a large plateau on the top that indicates that the weight of the asymmetric fission mode is almost comparable with that of the symmetric fission mode. In the case of fission of ^{250}Cf at $E^* = 46$ MeV (Fig. 5), the measured secondary charge and mass distributions demonstrate the conservation of the asymmetric components [9]. The experimental width of the charge distribution extends at FWHM over 16 charge numbers. Note that in the case of

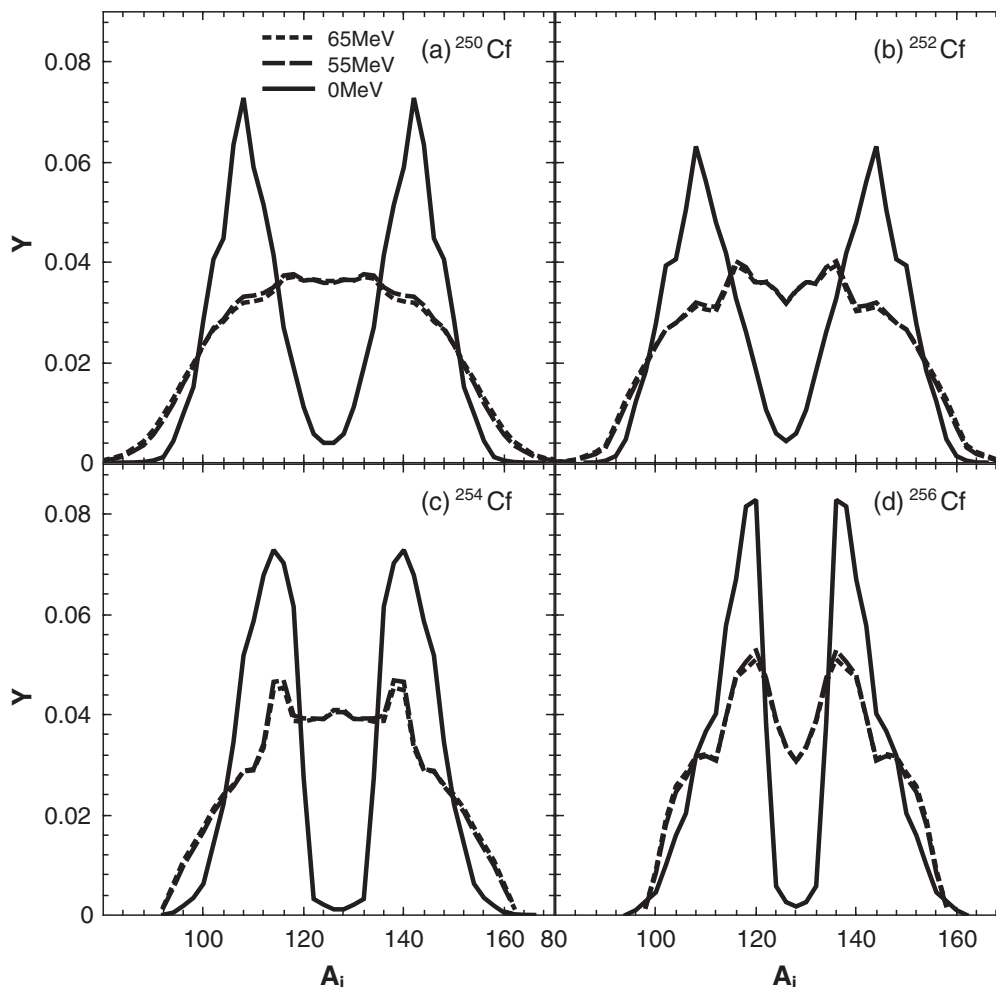


FIG. 9. The calculated mass distributions of fragments resulting from the fission of (a) ^{250}Cf , (b) ^{252}Cf , (c) ^{254}Cf , (d) ^{256}Cf at the indicated excitation energies. The calculations are performed for the even-even mass and charge fragmentations.

fissioning $^{204-208}\text{Rn}$, $^{210-218}\text{Ra}$, and ^{222}Th with the symmetric nature of fission, the width of the measured distribution is eight units at FWHM [16].

The charge distribution resulting from the fission of ^{248}Cf at excitation energy in the range between 25 and 35 MeV display both almost symmetric Cd + Sn and asymmetric Ru + Xe modes with relatively equal weights (Fig. 3). Thus, the transition from two-peaked to four-peaked charge distribution occurs with increasing excitation energy. This behavior is not found for other californium nuclei, even at higher excitation energies.

The fast evolution of the symmetric component observed with increasing excitation energy from 0 to (15–25) MeV can be attributed to the fast shell melting of the magic (Sn) and near magic (Cd) nuclei. At low excitation energies, the stiffness of the nuclei provide a spherical shape for the two nuclei of almost symmetric configuration Cd + Sn, which leads to a larger value of the interaction potential, and, correspondingly, to a larger value of the total potential energy U , compared to the more asymmetric Mo + Ba or Ru + Xe configurations. As the excitation energy is increased the shell effects wash away and the lowering nuclear stiffness provide a softer symmetric configuration, in which the value of U decreases (the decrease

in the Coulomb term of the LD potential and the decrease of the interaction potential is not compensated by the increase of the surface energies of the two nuclei), leading to higher yields. In this way one can understand the shift to more symmetric mass and charge distributions with increasing E^* .

As seen in Figs. 3, 9, and 10, there is the difference between the shapes of mass and charge yields in the fission of ^{248}Cf at $E^* = 45$ MeV and ^{252}Cf at $E^* = 55-65$ MeV. For fission of $^{248,252}\text{Cf}$, the pronounced asymmetric mass distributions of fission fragments, coexist with the charge distributions with almost symmetric peak at Cd + Sn.

The saturation of the symmetric mass and charge components with increasing excitation energy (Figs. 9 and 10) can be understood in the following way. For each mass and charge fragmentation, the configurations with the highest yields correspond to local minimum on the potential energy surface (β_L, β_H). This minimum on the potential energy surface (PES) results from the competition between the macroscopic interaction and liquid-drop energies, and the macroscopic shell corrections at scission. The strong shells also affect the macroscopic parts of the potential energy by keeping the minimum energy at small deformations (β_L, β_H). With increasing excitation energy, the shell effects are washed out and the

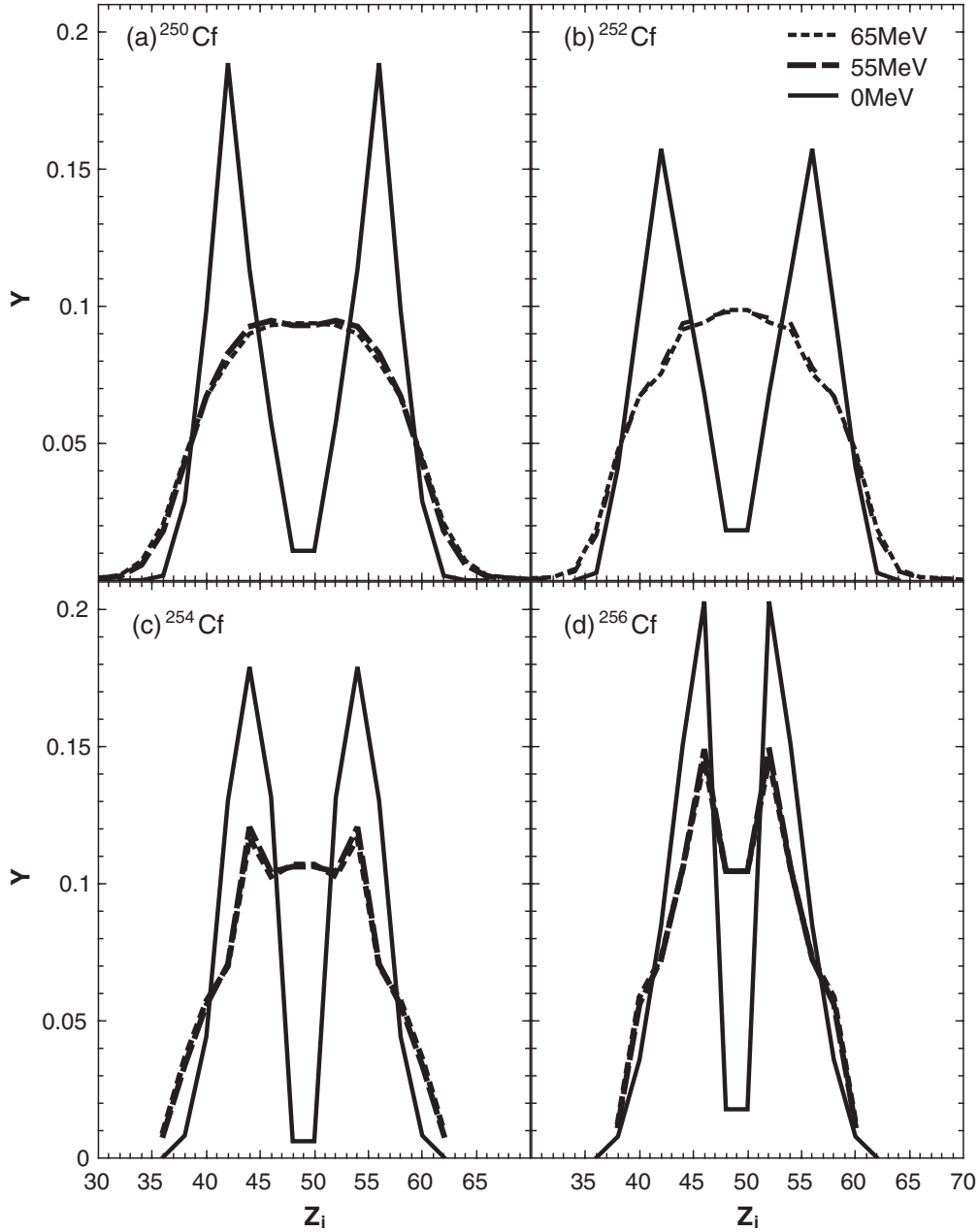


FIG. 10. The calculated charge distributions of fragments resulting from the fission of (a) ^{250}Cf , (b) ^{252}Cf , (c) ^{254}Cf , (d) ^{256}Cf at the indicated excitation energies. The calculations are performed for the even-even mass and charge fragmentations.

stiffness k_i of the nuclear surface decreases. At the same time the temperature-dependent terms of the macroscopic part of U begins to act stronger on the PES. The combined effect is the enlargement of the minimum on the PES and its shift towards larger deformations. At large E^* , the shell effects are completely damped, the surface stiffness becomes minimal, and the minima on the PES reach their maximum widths and final positions dictated by the macroscopic part of U . At this point the yields reach the maximal values, and further increase of excitation energy leads only to the population of more asymmetric accessible (by the total energy conservation) configurations. Note that the width of the minimum is mainly governed by the stiffness parameters of two nuclei—a large

k_i value provides a narrow and deep minimum, while a small k_i value leads to a wide and shallow minimum. In Fig. 11, the example of the increase of the width of the PES minimum with increasing excitation energy is presented for the $^{108}\text{Mo} + ^{142}\text{Ba}$ fragmentation of the ^{250}Cf nucleus at $E^* = 0, 15, 25, 35,$ and 45 MeV. This fragmentation corresponds to the maxima of the charge and mass distributions in the spontaneous and thermal-neutron-induced fission of ^{250}Cf . At given E^* , the scission configurations with the potential energies in the range between the minimum value of $U = U_{\min}(E^*)$ and $U = U_{\min}(E^*) + 2$ MeV are enclosed in contour lines. The inspection of Eq. (5) reveals that these configurations provides the highest yields. As seen, the minimum on the PES becomes

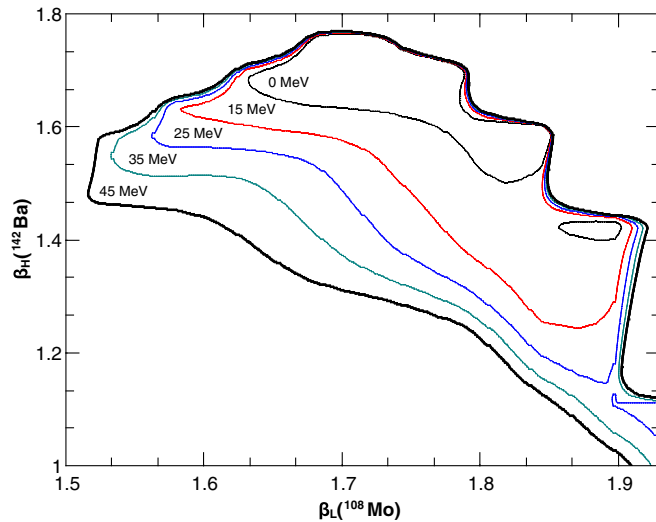


FIG. 11. The scission configurations with the potential energies between U_{\min} and $U_{\min} + 2$ MeV are enclosed in contour lines on plane (β_L, β_H) for the fragmentation $^{250}\text{Cf} \rightarrow ^{108}\text{Mo} + ^{142}\text{Ba}$ at indicated E^* .

wider and shallower with increasing E^* . There is saturation of the expansion of this minimum at $E^* > 35$ MeV.

In Table I, the calculated average charge $\langle Z \rangle$ and mass $\langle A \rangle$ numbers of the light fragments resulting from the fission of cold and excited even-even isotopes $^{248-256}\text{Cf}$ are presented. The values of $\langle Z_L \rangle$ and $\langle A_L \rangle$ weakly increase with E^* up to ≈ 25 MeV and almost unchangeable at higher energies. Such behavior is a reflection of the increase of the symmetric yields compared to the asymmetric ones. It is worth to note that stabilization of $\langle Z_L \rangle$ and $\langle A_L \rangle$ is related to the saturation of the widths of the PES minima with E^* . So, we do not expect that with increasing excitation energy the distributions are only peaked around $(Z_{CN}/2, A_{CN}/2)$, but reach a maximum height at certain value of E^* and then become wider with increasing E^* . The same behavior is found in Ref. [18]. In Table I, the peak-to-valley ratios of the charge and mass distributions decrease towards the values $\approx 1-1.5$, pointing out again a saturation of these distributions.

IV. CONCLUSIONS

The mass and charge distributions resulting from the spontaneous and induced fission of even-even nuclei $^{248-256}\text{Cf}$ were calculated within the statistical scission-point fission model. For these fissioning nuclei, the available experimental mass distributions in the spontaneous and thermal-neutron-induced fission were well described. As a global trend, the mass and charge yields are symmetrized with increasing excitation energy and decreasing isospin. In the fission of $^{248-256}\text{Cf}$ at excitation energy about of 55 MeV, the saturation of the

TABLE I. The calculated average charge $\langle Z \rangle$ and mass $\langle A \rangle$ numbers of the light fission fragments, and peak-to-valley ratios $P/V(Z)$ and $P/V(A)$ of the charge and mass distributions, respectively, in the fission of even-even nuclei $^{248-256}\text{Cf}$ at different excitation energies E^* (Figs. 3–8).

Fissioning nucleus	E^* (MeV)	$\langle Z \rangle$	$\langle A \rangle$	$P/V(A)$	$P/V(Z)$
^{248}Cf	0	43.6	110.0	42.5	27.1
	15	44.4	114.7	1.8	2.9
	25	44.6	116.2	1.2	1.9
	35	44.6	116.7	1.0	1.5
	45	44.6	116.8	0.9	1.4
^{250}Cf	0	42.4	110.3	17.4	18.4
	15	43.1	113.3	2.3	2.5
	25	43.3	114.1	1.4	1.5
	35	43.4	115.0	1.2	1.2
	45	43.4	115.2	1.1	1.0
^{252}Cf	0	42.5	109.4	8.6	14.7
	15	43.2	113.3	1.7	2.2
	25	43.4	114.1	1.3	1.5
	35	43.4	115.0	1.1	1.4
	45	43.4	115.2	1.0	1.3
^{254}Cf	0	43.1	112.7	29.2	63.2
	15	44.0	114.3	2.1	2.4
	25	44.1	114.5	1.6	1.7
	35	44.1	114.5	1.3	1.4
	45	44.1	114.5	1.2	1.2
^{256}Cf	0	42.5	115.0	11.4	48.3
	15	44.7	119.6	2.0	2.8
	25	44.7	120.0	1.7	2.2
	35	44.7	120.0	1.6	1.9
	45	44.7	120.0	1.5	1.8

symmetric component was found. As predicted, the charge distribution resulting from the fission of ^{248}Cf at excitation energies in the range between 25 and 35 MeV shows both almost symmetric (Cd + Sn) and asymmetric (Ru + Xe) modes with relatively equal weights. In the fission of ^{248}Cf at $E^* = 45$ MeV and ^{252}Cf at $E^* = 55-65$ MeV, the difference was predicted between the shapes of mass (the pronounced asymmetric component) and charge (almost symmetric component Cd + Sn) yields.

ACKNOWLEDGMENTS

This work was partially supported by the Romania-JINR(Dubna) Cooperation Programme, the Russian Foundation for Basic Research (17-52-12015, 17-52-45037) and DFG (Bonn), Contract No. Le439/16. The work of N.V.A. was supported by Tomsk Polytechnic University Competitiveness Enhancement Program grant.

- [1] U. Brosa, S. Grossmann, and A. Müller, *Phys. Rep.* **197**, 167 (1990).
 [2] I. V. Ryzhov *et al.*, *Phys. Rev. C* **83**, 054603 (2011).
 [3] J. King *et al.*, *Eur. Phys. J. A* **53**, 238 (2017).

- [4] V. Simukhin, Ph.D. thesis, Uppsala University, 2010; I. V. Ryzhov *et al.*, *J. Korean Phys. Soc. C* **59**, 1864 (2011); V. Simukhin *et al.*, *Nucl. Data Sheets* **119**, 331 (2014).

- [5] H. Naik, T. N. Nathaniel, A. Goswami, G. N. Kim, M. W. Lee, S. V. Suryanarayana, S. Ganesan, E. A. Kim, M.-H. Cho, and K. L. Ramakumar, *Phys. Rev. C* **85**, 039905(E) (2012); H. Naik *et al.*, *ibid.* **85**, 024623 (2012); *Nucl. Phys. A* **913**, 185 (2013); **941**, 16 (2015); **952**, 100 (2016).
- [6] A. Deppman, E. Andrade-II, V. Guimarães, G. S. Karapetyan, and N. A. Demekhina, *Phys. Rev. C* **87**, 054604 (2013); A. Deppman, E. Andrade-II, V. Guimarães, G. S. Karapetyan, A. R. Balabekyan, and N. A. Demekhina, *ibid.* **88**, 024608 (2013); A. Deppman *et al.*, *ibid.* **88**, 064609 (2013).
- [7] M. Caamaño *et al.*, *Phys. Rev. C* **88**, 024605 (2013).
- [8] C. Rodríguez-Tajes, F. Farget, X. Derkx, M. Caamaño, O. Delaune, K.-H. Schmidt, E. Clément, A. Dijon, A. Heinz, T. Roger, L. Audouin, J. Benlliure, E. Casarejos, D. Cortina, D. Doré, B. Fernández-Domínguez, B. Jacquot, B. Jurado, A. Navin, C. Paradela, D. Ramos, P. Romain, M. D. Salsac, and C. Schmitt, *Phys. Rev. C* **89**, 024614 (2014).
- [9] D. Ramos *et al.*, *Phys. Rev. C* **97**, 054612 (2018); **99**, 024615 (2019).
- [10] R. Léguillon *et al.*, *Phys. Lett. B* **761**, 125 (2016).
- [11] K. Hirose *et al.*, *Phys. Rev. Lett.* **119**, 222501 (2017).
- [12] J. P. Unik *et al.*, in *Physics and Chemistry of Fission*, Vol. II (IAEA, Vienna, 1974), p. 25.
- [13] C. Romano, Y. Danon, R. Block, J. Thompson, E. Blain, and E. Bond, *Phys. Rev. C* **81**, 014607 (2010).
- [14] H. Paşca, A. V. Andreev, G. G. Adamian, and N. V. Antonenko, *Eur. Phys. J. A* **54**, 104 (2018).
- [15] M. D. Chadwick *et al.*, *Nucl. Data Sheets* **112**, 2887 (2011).
- [16] H. Paşca, A. V. Andreev, G. G. Adamian, and N. V. Antonenko, *Phys. Lett. B* **760**, 800 (2016).
- [17] H. Paşca, A. V. Andreev, G. G. Adamian, and N. V. Antonenko, *Phys. Rev. C* **94**, 064614 (2016).
- [18] H. Paşca, A. V. Andreev, G. G. Adamian, and N. V. Antonenko, *Phys. Rev. C* **97**, 034621 (2018).
- [19] H. Paşca, A. V. Andreev, G. G. Adamian, and N. V. Antonenko, *Nucl. Phys. A* **969**, 226 (2018).
- [20] B. D. Wilkins, E. P. Steinberg, and R. R. Chasman, *Phys. Rev. C* **14**, 1832 (1976).
- [21] T. Matsuse, C. Beck, R. Nouicer, and D. Mahboub, *Phys. Rev. C* **55**, 1380 (1997).
- [22] S. J. Sanders, A. Szanto de Toledo, and C. Beck, *Phys. Rep.* **311**, 487 (1999).
- [23] S. Panebianco, J.-L. Sida, H. Goutte, J.-F. Lemaître, N. Dubray, and S. Hilaire, *Phys. Rev. C* **86**, 064601 (2012).
- [24] M. Caamaño *et al.*, *Phys. Rev. C* **92**, 034606 (2015).
- [25] A. V. Andreev, G. G. Adamian, N. V. Antonenko, S. P. Ivanova, and W. Scheid, *Eur. Phys. J. A* **22**, 51 (2004); **26**, 327 (2005); A. V. Andreev, G. G. Adamian, and N. V. Antonenko, *Phys. Rev. C* **86**, 044315 (2012); A. V. Andreev, G. G. Adamian, N. V. Antonenko, and A. N. Andreyev, *ibid.* **88**, 047604 (2013).
- [26] G. G. Adamian, N. V. Antonenko, and W. Scheid, *Clusters in Nuclei*, Vol. 2, edited by C. Beck (Springer-Verlag, Berlin, 2012), p. 165.
- [27] H. Paşca, A. V. Andreev, G. G. Adamian, N. V. Antonenko, and Y. Kim, *Phys. Rev. C* **93**, 054602 (2016); H. Paşca, *EPJ Web Conf.* **107**, 07003 (2016).
- [28] H. Paşca, A. V. Andreev, G. G. Adamian, and N. V. Antonenko, *Eur. Phys. J. A* **52**, 369 (2016).
- [29] J. Maruhn and W. Greiner, *Z. Phys.* **251**, 431 (1972).
- [30] G. G. Adamian *et al.*, *Int. J. Mod. Phys. E* **05**, 191 (1996).
- [31] G. Sauer, H. Chandra, and U. Mosel, *Nucl. Phys. A* **264**, 221 (1976).
- [32] J. P. Balagna *et al.*, *Phys. Rev. Lett.* **26**, 145 (1971).
- [33] D. C. Hoffman, J. B. Wilhelmy, J. Weber, W. R. Daniels, E. K. Hulet, R. W. Loughheed, J. H. Landrum, J. F. Wild, and R. J. Dupzyk, *Phys. Rev. C* **21**, 972 (1980).
- [34] C. E. Bemis *et al.*, *Phys. Rev. C* **15**, 705 (1977).
- [35] G. M. Ter-Akopian *et al.*, *Phys. Rev. C* **55**, 1146 (1997).